A hybrid deterministic-probabilistic approach to model the mechanical response of helically arranged hierarchical strands

A *hybrid* probabilistic-deterministic approach to model the mechanical response of helically arranged hierarchical strands

M. Fraldi[1,2,3], G. Perrella[1], M. Ciervo[4], F. Bosia[4] and N.M. Pugno[5,6,7*]

[1]Department of Structures for Engineering and Architecture, University of Napoli Federico II - Italy
[2]Interdisciplinary Research Center for Biomaterials, University of Napoli Federico II - Italy
[3]Institute of Applied Sciences and Intelligent Systems, National Research Council - Italy
[4]Department of Physics and Nanostructured Interfaces and Surfaces Centre, University of Turin - Italy
[5]Department of Civil, Environmental and Mechanical Engineering, University of Trento - Italy
[6]Centre of Materials and Microsystems, Bruno Kessler Foundation, Trento, Italy
[7]School of Engineering and Materials Science, Queen Mary University, London, UK

Abstract

Very recently, a Weibull-based probabilistic strategy has been successfully applied to bundles of wires to determine their overall stress-strain behaviour, also capturing previously unpredicted nonlinear and post-elastic features of hierarchical strands. This approach is based on the so-called "Equal Load Sharing (ELS)" hypothesis by virtue of which, when a wire breaks, the load acting on the strand is homogeneously redistributed among the surviving wires. Despite the overall effectiveness of the method, some discrepancies between theoretical predictions and *in silico* Finite Element-based simulations or experimental findings might arise when more complex bundle structures are analysed, e.g. helically arranged bundles. To overcome these limitations, an enhanced *hybrid* approach is proposed in which the probability of rupture is combined with a deterministic mechanical model of a strand constituted by helically-arranged and hierarchically-organized wires. The results show that generalized stress-strain responses - incorporating tensile/torsion coupling - are naturally found and, once one or more elements break, the competition between geometry and mechanics of the strand microstructure, i.e. the different cross sections and helical angles of the wires belonging to the different hierarchical levels of the strand, determines the no longer homogeneous stress redistribution among the surviving wires whose fate is hence governed by an "*Unequal* Load Sharing" criterion.

1. Introduction

Fibre Bundle Models (FBM) were first introduced in the 1920s and first comprehensively developed by Daniels about twenty years later (Daniels, 1945) to describe failure processes in a large number of materials and settings, the success of the approaches depending on their relative simplicity, the clear underlying physics and the capability of preserving some key aspects which ensured to catch with sufficient richness the overall mechanical behaviour of the structures. Essentially, at a certain scale the material is modelled as a network of fibres, arranged in parallel and/or in series and subject to uniaxial force, with failure mechanisms governed by a statistical (Weibull) distribution of wire yield strengths. Therefore, an equal load sharing hypothesis is assumed and, when fibres progressively fracture or reach a stress threshold as the external load increases, the stresses are redistributed uniformly among the remaining fibres in the bundle

* Corresponding author: prof. Nicola M. Pugno, nicola.pugno@unitn.it

(Pradhan, 2010). This type of model allows the study of fracture processes evaluating statistical fluctuations, rather than average values. Thus, FBMs have been used as numerical tools to describe phenomena such as creep and fatigue, but also failure processes in networks, traffic jams, or earthquakes. In particular, recently, the topic has enjoyed renewed interest due on one hand to more advanced computational tools, and on the other to the study of biological materials, which very often exhibit a fibre-based structure (Meyers, 2008). In fact, a large number of biomaterials are inherently hierarchical, often including several hierarchical scale levels, as one can for instance observe in tendons or in spider silk. In many cases these natural materials have been found to display exceptional simultaneous strength and toughness characteristics, which are hard to replicate in artificial media (Ritchie, 2011). Various mechanisms contribute to confer enhanced and somehow optimal mechanical behaviours to these classes of hierarchically organized biomaterials, including strategic sacrificial bonds, efficient arrangements of the reinforcements for crack deviation, crack bridging effects, as well as multiscale energy dissipation mechanisms. Attempts have been made to replicate these toughening effects in artificial fibres, e.g. using knots as energy dissipators (Pugno, 2014; Bosia, 2016). To model toughening mechanisms in fibre bundles or textiles, one however needs to correctly reproduce effects related to the hierarchical organization and hierarchical implementations of FBMs have been to this purpose presented in the literature (Pugno, 2008). Additionally, complex structural arrangements can arise, e.g. helically arranged fibres around a central fibre or bundle. Although fibre twisting and friction can be taken into account phenomenologically in a FBM, as done in (Pan, 1993) and (Pugno, 2012), this approach requires the introduction of additional parameters that need to be derived experimentally or theoretically. However, the validity of the Equal Load Sharing (ELS) hypothesis cannot completely capture some emerging failure mechanisms, nonlinear generalized stress-strain behaviours and torsion-elongation coupling in presence of complex hierarchical, interwoven fibre bundles. As a consequence, with the aim of updating the previously mentioned models and starting from the idea of considering statistical Weibull-like distributions of mechanical properties for the wires, here we propose a bottom-up approach to first trace the actual role played by helical arrangements in hierarchical bundles (or strands), for finally combining *ad hoc* new theoretical findings with the ELS-based insights and outcomes to build up a hybrid probabilistic-deterministic model.

2. Mechanics of the wires and overall strand response

Within the general framework of the theory of naturally curved rods by Love (1944), we derive here a mechanical model able to predict the response of simple as well as hierarchical strands, subject to overall prescribed load or displacement boundary conditions. In particular, self-equilibrating tensile axial forces F and torques M_t exerted at the strand extremities will be considered, together with the corresponding generalized overall deformations, represented by the elongation ε and the torsion per unit length, φ. The resulting constitutive relations for the strand are then explicitly derived on the basis of selected key geometrical and mechanical parameters. In the case of a multilayered straight strand these parameters are, for each generic $i-th$ layer, the wire helix angle α_i, the radii of the wire cross sections R_i, the helix radius r_i, the number of wires N_i, and the Young's moduli, Poisson ratios and stress thresholds of the constituent materials.

With reference to the mechanics of a generic straight strand structure, namely a Multi-layered Straight Strand (MSS) constituted by a central core surrounded by a number of layers made of helically wound wires, let us consider a cylindrical reference system with coordinates $\{r, t, z\} \in \mathbb{R}^3$, z being the strand axis (see Figure 1A). By following the approach suggested by Love (1944), an additional helical reference system, based on a Cartesian coordinate system whose unit vectors are

$\{\boldsymbol{e}_1, \boldsymbol{e}_2, \boldsymbol{e}_3\}$, is locally placed over the generic cross section of each wire. In particular, the unit vector $\boldsymbol{e}_3$ is tangent to the wire centreline, while the unit vector $\boldsymbol{e}_2$ is chosen to be normal to the $\boldsymbol{e}_1 - \boldsymbol{e}_3$ plane where the helical wire centreline lies and bending is expected during the deformation. Here, a MSS made of $m \in \mathbb{N}$ layers, each of which constituted by $N_i \in \mathbb{N}$ wires, with $i \in \{1, 2, ..., m\}$, is adopted as a basic scheme to introduce the kinematics of the strand model unit, from which hierarchically organized structural configurations of growing complexity can be conceived. The layers are thus numbered so that $i = 1$ is the inner core wire, while $i = m$ indicates the external layer. In this way, the MSS configuration represents the generic wire arrangement in a straight strand. However, simple straight strands with a single layer of wires (i.e. made by a central core surrounded by a six-wire layer, see Figure 1B), as well as multiple-core strands characterized by the assembly of several straight strands, can also be studied by following the same strategy proposed below and therefore the obtained results can be straightforwardly generalized to more complex hierarchical strand microstructures (see Figure 1C). Each generic MSS $i-th$ layer is made by wires having circular cross sections with radii R_i, wrapped helically around the $(i-1)-th$ inner layer, with helix radius

$$r_i = \sum_{j=1}^{i+1} 2R_j - (R_{i+1} + R_1), \quad \forall i \geq 1 \tag{1}$$

All the wires of the $i-th$ layer are assumed to lie in the same initial helical configuration, and the helix angle α_i refers to the normal to the strand cross-section. Additionally, two further parameters are introduced for computational convenience, e.g. the complementary angle $\beta_i = \pi/2 - \alpha_i$, measured with respect to the strand axis, and the helix pitch of the outer wires in the strand, $p_i = 2\pi\, r_i \tan\alpha_i$.

In modelling the strand, some key geometrical and mechanical assumptions are introduced, essentially following the idea by Costello (Costello, 1976). First, the overall strand length is assumed to sufficiently large to avoid end effects. Furthermore, it is assumed that the wires of a generic layer do not touch each other but all of them are in contact with the adjacent layers. Friction between wires and core and among adjacent layers is hence hypothesized to be sufficient to avoid any relative slip, and interlayer pressure effects and contact deformations are instead taken into account.

From the mechanical point of view, the strands are assumed to exhibit linear elastic behaviour up to a prescribed threshold, say the yield stress, then progressively going toward increasing strains at constant stress, as happens in standard (perfect) plasticity. Alternatively, for a selected stress threshold, an elastic-brittle law will be also considered for describing the post-elastic mechanical behaviour of the wires, as actually implemented through a stepwise procedure in the considered examples to compare theoretical and numerical results. It is worth highlighting that further dissipative phenomena such as inter-wire slipping, wire flattening and plastic deformations at the layer interfaces are instead neglected. In this respect, however, Utting and Jones (Utting and Jones, 1987), by focusing their attention on inter-wire friction of a strand in the case of small deformations, showed experimental results which demonstrated a small influence of such effects on the global strand behaviour. Also, Nawrocki and Labrosse (Nawrocki and Labrosse, 2000) performed studies on inter-wire contacts, by using Finite Element numerical models, highlighting that rolling and sliding might influence the overall mechanical response of strands through pivoting

between wires of adjacent layers. Nevertheless, comparisons of the results of numerical analyses and experimental data seems to suggest that pivoting is a stress-free phenomenon, at least for small and moderately large deformations, thus allowing to neglect these local effects and to simply relate wire kinematics to the overall degrees of freedom of the strand. As a consequence, according to the theory of rods, a single wire reacts to overall loads (macroscopically applied to the strand) exhibiting a combined deformation regime characterized by local elongation, bending and twisting. All the strand filaments are thus assumed to be isotropic and linearly elastic (until a prescribed limit stress value), with Young's moduli, E_i, and Poisson ratios, ν_i, "i" still denoting the wire material of the generic $i-th$ layer. Equivalently, corresponding Lamé moduli, $\lambda_i = \nu_i E_i \times [(1+\nu_i)\times(1-2\nu_i)]^{-1}$ and $2\mu_i = E_i \times (1+\nu_i)^{-1}$, will be also introduced below for calculus convenience.

2.1. Kinematics at the wire level

Neglecting overall bending of the structure (i.e. the resultant bending moment at the extremities), it is possible to completely describe the global deformation of a strand through two generalized strain measures, that is the strand axial elongation

$$\varepsilon = \frac{L - L_0}{L_0} \tag{2}$$

and the strand torsion, defined as twist angle per strand unit length as follows

$$\varphi = \frac{\Delta\Theta}{L_0} \tag{3}$$

where L_0 and L respectively refer to the strand length in initial and stressed configurations and $\Delta\Theta$ denotes the relative twist angle between two strand cross sections at a distance L_0.

Therefore, starting from the Ramsey wire rope theory (Ramsey, 1988; Ghoreishi, 2007), it is possible to construct a model that allows to take into account the deformation due to the inter-wire contact driven by the Poisson's ratio effect, including local phenomena into the overall strand kinematics, as described in detail below.

In the local helical reference system whose unit vectors are $\{\boldsymbol{e}_1, \boldsymbol{e}_2, \boldsymbol{e}_3\}$ (see Figure 1A) the unstrained (natural) curvatures of the wires in the generic layer of the strand can be defined as follows

$$\kappa_{i0} = 0, \quad \kappa'_{i0} = \frac{\cos^2 \alpha_i}{r_i} \tag{4}$$

where κ_{i0} and κ'_{i0} are the curvatures in the planes whose normals are $\boldsymbol{e}_1$ and $\boldsymbol{e}_2$, respectively, while the axial twist around $\boldsymbol{e}_3$ is

$$\tau_{i0} = \frac{\sin \alpha_i \cos \alpha_i}{r_i} \tag{5}$$

As the strand is loaded, each wire assumes a deformed helical configuration coaxial with the initial helix (Costello 1990). The updated curvatures and twist therefore take the form

$$\kappa_{iD} = 0 \quad \kappa'_{iD} = \frac{\cos^2 \alpha_{iD}}{r_{iD}}, \quad \tau_{iD} = \frac{\sin \alpha_{iD} \cos \alpha_{iD}}{r_{iD}} \tag{6}$$

where r_{iD} and α_{iD} are the radius and the angle of the deformed helix of the wires belonging to the $i-th$ layer. It is worth noticing that, because no overall bending is applied to the strand, curvature κ_{i0} in the plane $\boldsymbol{e}_2 - \boldsymbol{e}_3$ and its related variation $\Delta\kappa_i = \kappa_{iD} - \kappa_{i0}$, both remain zero in every section. Small strand deformations imply that $\{\varepsilon, \Delta\Theta\} << 1$ and consequently second order terms can be neglected in the calculations. According to the general theory of thin rods (Love 1944), helix angle increment $\Delta\alpha_i = \alpha_{iD} - \alpha_i$ and axis wire elongation ε_i can be related to the global strand deformations, ε and φ, through the following equation

$$\varphi = \frac{\varepsilon_i}{\tan \alpha_i} - \Delta\alpha_i + \frac{\sum_{j=i}^{i+1} 2\nu_j R_j \varepsilon_j - (\nu_i R_i \varepsilon_i + \nu_1 R_1 \varepsilon)}{r_i \tan \alpha_i} \tag{7}$$

which is the relation that accounts for the coupling effect between torsion and elongation along the strand axis. Following the approach proposed by Costello (Costello 1990), the kinematics of the single wires is fully defined through three parameters: the local elongation ε_i measured along the wire axis, the local difference in wire curvature $\Delta\kappa'_i$ in the plane $\boldsymbol{e}_2 - \boldsymbol{e}_3$ and the wire twist angle variation $\Delta\tau_i$. Finally, the linearization obtained by taking only the first order the terms $\{\varepsilon, \Delta\alpha_i\}$ in the strain measures gives the wire elongation along its axis as

$$\varepsilon_i = \varepsilon - \frac{\Delta\alpha_i}{\tan \alpha_i} \tag{8}$$

and the wire bending curvature in the $\boldsymbol{e}_1 - \boldsymbol{e}_3$ plane, $\Delta\kappa'_i = \kappa'_{iD} - \kappa'_{i0}$, becomes

$$\Delta\kappa'_i = -\frac{2 \sin \alpha_i \cos \alpha_i}{r_i} \Delta\alpha_i + \frac{\sum_{j=1}^{i+1} 2\nu_j R_j \varepsilon_j - (\nu_i R_i \varepsilon_i + \nu_1 R_1 \varepsilon)}{r_i} \times \frac{\cos^2 \alpha_i}{r_i} \tag{9}$$

while the wire torsion $\Delta\tau_i = \tau_{iD} - \tau_{i0}$ takes the form

$$\Delta\tau_i = \frac{1 - 2\sin^2 \alpha_i}{r_i} \Delta\alpha_i + \frac{\sum_{j=1}^{i+1} 2\nu_j R_j \varepsilon_j + (\nu_i R_i \varepsilon_i + \nu_1 R_1 \varepsilon)}{r_i} \times \frac{\sin \alpha_i \cos \alpha_i}{r_i} \tag{10}$$

As a result of the assumed kinematics and due to the Poisson's ratio effect, the radial deformation δr_i of the helix radius r_i can finally be expressed as follows

$$\delta r_i = 1 - \frac{r_{iD}}{r_i} = \frac{\sum_{j=i}^{i+1} 2\nu_j R_j \varepsilon_j - (\nu_i R_i \varepsilon_i + \nu_1 R_1 \varepsilon)}{\sum_{j=1}^{i+1} 2R_j - (R_i + R_1)} \tag{11}$$

where, for the MSS, the local core strain value is taken to be coincident with the global ones, that is $\varepsilon_1 \equiv \varepsilon$.

2.2. Equilibrium and generalized stress-strain constitutive relations at the wire level

With respect to the equilibrium, three components of the resulting forces can be traced on each wire cross section of the generic $i-th$ layer: two shear components directed along the $\boldsymbol{e}_1$ and $\boldsymbol{e}_2$ directions, say S_i and S'_i, respectively, and the tensile force, T_i, along $\boldsymbol{e}_3$ (see Figure 1A). Furthermore, three resulting moments (two bending moments and a torque) also emerge on the wire cross sections, two lying respectively in the planes whose normals are $\boldsymbol{e}_1$ and $\boldsymbol{e}_2$, say G_i and G'_i, and the torsion H_i acting on the cross section plane. In the present case, the shear force S_i vanishes since $\kappa_{i0} = 0$, as does the bending moment G_i because $\kappa_{iD} = 0$. Also, although classical body forces are neglected, the contact forces per centreline unit length X_i at the interfaces between wires and adjacent layers play the role of body forces directed along the $\boldsymbol{e}_1$ direction, appearing *de facto* within the field equations. Within these hypotheses, the equilibrium equations referred to the helical wire centreline can be written as

$$\begin{cases} -S'_i \tau_{iD} + T_i \kappa'_{iD} + X_i = 0 \\ -G'_i \tau_{iD} + H_i \kappa'_{iD} - S'_i = 0 \end{cases} \tag{12}$$

By following Ramsey (Ramsey, 1988), the constitutive relations between the nonzero generalized forces and the components of curvature, twist, and elongation give

$$G'_i = E_i I_i \times \left(\Delta\kappa'_i + \kappa'_{i0} \varepsilon_i \right), \quad H_i = \mu_i J_i \times \left(\Delta\tau_i + \tau_{i0} \varepsilon_i \right), \quad T_i = E_i A_i \varepsilon_i \tag{13}$$

where $I_i = \pi R_i^4 / 4$ is the cross-sectional moment of inertia with respect to the $\boldsymbol{e}_2$ axis, $J_i = \pi R_i^4 / 2$ is the polar moment of inertia of the cross section of the wire, and $A_i = \pi R_i^2$ represents the wire cross-sectional area, μ_i and E_i are the already introduced first Lamé and Young moduli of the wire, respectively. The resultant axial force F^i and the twisting moment M_t^i emerging from the generic layer of the strand comprising the helical wires are thus respectively given by

$$F^i = N_i \times \left(T_i \sin\alpha_i + S'_i \cos\alpha_i \right) \tag{14}$$

and

$$M_t^i = N_i \times \left(H_i \sin\alpha_i + G'_i \cos\alpha_i + T_i r_i \cos\alpha_i - S' r_i \sin\alpha_i \right) \tag{15}$$

where N_i is the already introduced number of wires in the layer.

2.3. Derivation of stresses at single wire level

Once the loads acting on the individual wires are known from Eqs. (12) and (13), it is possible to determine the stress associated with these loads. By starting from the assumption that the wires are initially stress-free, the normal stress induced by the tensile force and acting on the wire cross-section of the generic $i-th$ layer is

$$\sigma_3^i = \frac{T_i}{\pi R_i^2} \tag{16}$$

whereas the maximum normal stress due to the bending moment G'_i is

$$\sigma_{\max}^i = \frac{4G'_i}{\pi R_i^3} \tag{17}$$

and the maximum shearing stress due to the twisting moment H_i is

$$\tau_{\max}^i = \frac{2H_i}{\pi R_i^3} \tag{18}$$

The stress generated by the shear force S'_i is in general negligible if compared with the others and, as a consequence, is not computed in the following calculations, for the sake of simplicity. The maximum values of the stresses found above will hence be considered to estimate the proximity of the stress state in a wire to the corresponding material stress threshold. In particular, in the following analyses, the stress components to be compared with the wire strength will be calculated as

$$\sigma^i \simeq \sigma_3^i + \frac{2}{3}\sigma_{\max}^i \tag{19}$$

$$\tau^i \simeq \frac{2}{3}\tau_{\max}^i \tag{20}$$

Due to the fact that the loads are applied at the sole strand extremities and no gradients are assigned to loads, stresses and strains in the wires can be taken as spatially constant along the direction associated to $\boldsymbol{e}_3$ in the local reference system, as well as with respect to the strand axis. Additionally, as suggested by Costello (Costello 1990), the wires belonging to the $i-th$ layer do not touch each other and this implies that, both in the analytical calculations and at each step of the numerical simulations, the following inequality must be verified for each strand layer

$$R_i \times \sqrt{1 + \frac{\tan^2\left(\frac{\pi}{2} - \frac{\pi}{N_i}\right)}{\sin^2 \alpha_i}} < r_i \tag{21}$$

2.4. Overall response of the strand

2.4.1 *Twisting-elongation coupling at the strand level*

In order to obtain constitutive equations for the strand under consideration, it is possible to derive external loads on it by projecting the sum of the wires forces and moments along the strand axis. In this way, the total axial force F and the resultant torque M_t can be directly related to the generalized strand deformations ε and φ, by introducing the following matrix form

$$\begin{bmatrix} F \\ M_t \end{bmatrix} = \begin{bmatrix} \sum_{i=1}^{m} F^i \\ \sum_{i=1}^{m} M_t^i \end{bmatrix} = \begin{bmatrix} \sum_{i=1}^{m} k_{\varepsilon\varepsilon}^i & \sum_{i=1}^{m} k_{\varepsilon\varphi}^i \\ \sum_{i=1}^{m} k_{\varphi\varepsilon}^i & \sum_{i=1}^{m} k_{\varphi\varphi}^i \end{bmatrix} \times \begin{bmatrix} \varepsilon \\ \varphi \end{bmatrix} \tag{22}$$

where the superscript i denotes the generic layer of the wires and the coefficients collected in the (2×2) matrix physically represent the strand stiffness components. The constitutive equation (22) is essential in practical problems because it allows to deal with both cases where force-prescribed and displacement-prescribed boundary conditions are implemented. Elongation-twisting coupling due to the presence of nonzero out-of-diagonal coefficients in the stiffness strand matrix reflects the actual situations that in a strand with helical microstructure elongation and torsion cannot be considered as separate or independent mechanisms. As a consequence, when axial forces are prescribed at the strand extremities, the deformation is generally characterized by elongation accompanied by twisting and, conversely, when elongation is assigned in a test, the strand is stressed by both tensile forces and torsion. Moreover, it must be stressed that the overall coupling between axial forces and torsion in the strand is the effect of an analogous coupling at the wire level, where the additional bending regime contributes to the kinematics. At this *local* microstructure scale level, the key geometrical parameters that play the main role in the deformation of the wire are the twisting angle α_i, the ratio R_i / r_i between wire and helix radii and the helix pitch.

2.4.2 *Sensitivity analyses for varying boundary conditions*

As in the case of the strand, boundary conditions applied in terms of prescribed forces or displacements strongly influence the mechanical response of the wire, also producing some counterintuitive or somehow unforeseeable effects in the deformation when axial wire elongation ε_i, helix curvature variations $\Delta\kappa'_i$ and wire torsion variation $\Delta\tau_i$ are plotted against the helical angle α_i. These results are illustrated for a simple straight strand in Figure 2 (the chosen example is a central core is surrounded by a six-wire layer), where - under the hypotheses of linear isotropic materials, small deformations and zero transversal contraction of the core ($\nu_1 = 0$) - two complementary limit cases are considered in which the same tensile axial forces are applied. In particular, in the first case, the twist at the ends is locked ($\varphi = 0, M_t \neq 0$), while in the second case the ends are torque-free ($\varphi \neq 0, M_t = 0$). The plots show how the three wire kinematical parameters, ε_2, $\Delta\kappa'_2$ and $\Delta\tau_2$, evolve with prescribed initial helix angle $\alpha_2 \in (0,\ \pi/2)$. Although geometrical compatibility requires a helical angle variation confined within

$\{\alpha_2 \in [\alpha_{2\min}, \pi/2[,\ \alpha_{2\min} \equiv \arctan\left[R_2/\left(\pi R_1 + \pi R_2\right)\right] > 0\}$, it is interesting to observe that wire elongation ε_2 always grows nonlinearly up to its upper bound, which coincides with the overall strand strain ε as $\alpha_2 \to \pi/2$, wire bending curvature $\Delta\kappa'_2$ exhibiting non-monotonic variations and wire twist $\Delta\tau_2$ displaying a nonlinear and non-monotonic trend which is also accompanied by an unexpected change in sign in the proximity of $\alpha_2 \cong \pi/4$, to accommodate the geometrical congruency due to the mutual interaction between local torsion and bending curvatures.
From the mechanical point of view, it is worth highlighting that the nonlinear and non-monotonic curves describing the variation of the wire strain measures - and in turn of the layer and of the overall strand kinematics - with the micro-structural parameters (in the example, the initial wire angle) can be of great interest in engineering applications. Indeed, since the local stress states are proportional to (or growing with) the strains, the above mentioned curves can be exploited to predict, as a function of the strand geometry, stress localization and peaks that otherwise could seemingly appear as bizarre, thus interpreting the way in which failure phenomena take place in bundles of wires with helical and hierarchical architectures and envisaging optimal strand design criteria.

3. The hybrid probabilistic-deterministic approach in strand failure: the *Unequal Load Sharing* (ULS) criterion

Following previous work by some of the authors (Bosia et al. 2012) and using the equations derived above for helically arranged microstructures, let us consider a generic strand made of a prescribed number of layers with a selected number of wires: each single wire can thus be stretched (and/or twisted) as a result of applied loads and/or displacements at the strand ends and observed to obey a linear elastic law up to its corresponding failure point, say until the stress threshold is attained. Its strength, here roughly assumed as the stress value at which the wire fails, can be determined from an equivalent stress value, σ_{eqv}, which, without loss of generality for the procedure at hand, is here referred to the von Mises yield criterion. As a consequence, for the generic $i-th$ wire one can write

$$\sigma^i_{eqv} = \sqrt{3J^i_2} = \sqrt{\left(\sigma^i\right)^2 + 3\left(\tau^i\right)^2} \tag{23}$$

where J^i_2 represents the second deviatoric stress invariant and the stress components are those derived in the Eqs. (19) and (20).
A probability distribution function can then be introduced in order to include the statistical variation in the failure mechanism of the strand for each wire under a prescribed stress state. For this purpose, it is assumed that the equivalent stress in the wire follows a Weibull distribution (Weibull, 1951), and that the wire failure strength is thus governed by the probability density function in the form

$$P\left(\sigma^i_{eqv}\right) = 1 - \exp\left[-\left(\sigma^i_{eqv}/\sigma^i_Y\right)^{\rho^i}\right] \tag{24}$$

where σ^i_Y is the reference stress threshold (*scale factor*) and ρ^i is the Weibull *shape factor* for the wire materials. Although behind of the scope of the present work, it is worth to highlight that Eq.

(24) implies that size dependent effects could be expected if one performs simulations of strands with prescribed structure at different scale levels.
Similarly to the cases of bundles analysed under the so-called “Equal Load Sharing (ELS)” hypothesis (Hemmer and Hansen 1992, Pugno 2012), when a wire of a hierarchically organized strand breaks, the load acting on the strand is redistributed among the surviving wires; however, contrary to the ELS stress reorganization, the above mentioned load is not redistributed in a homogenous (uniform) way among the constituents: the wires belonging to each layer, at the several hierarchical levels, are in fact subjected to different stress states as a consequence of the mechanics of the MSS illustrated in detail in the previous sections. Therefore, while the probabilistic approach - in the literature applied to bundles made of straight, although hierarchically organized, wires (Pugno 2012) - describes the collapse of one or more structural constituents by implying that a *homogeneous* redistribution of stresses within the surviving structure occurs, in the proposed approach the failure - and in turn the stress reorganization - is the result of the influence of the *probability* of rupture in the *deterministic* (inhomogeneous) distribution of stresses among the wires, governed by the mechanical model of strands constituted by helically arranged and hierarchically organized wires. As a result, once one or more elements break, the criterion of stress redistribution is ruled by the geometry and the mechanics of the strand microstructure and the redistribution of stresses among the surviving wires and their fates are no longer homogeneous, thus leading to a sort of "Unequal Load Sharing" *effect*, rather than *hypothesis*. In particular, by considering a prescribed deformation state of a generic $i-th$ layer in the strand in which one of the wires breaks (for the sake of simplicity brittle behaviour with no plastic deformation is assumed here), the total loads (14) and (15) are obtained as the sum of the forces acting on the remaining $N_i - 1$ wires. In a generic deformed state $\{\varepsilon, \varphi\}$, the total load that a strand can sustain is thus derived from the total number of intact fibres among the wires by virtue of the following relation

$$\exp\left[-\left(\sigma_{eqv}^{i}/\sigma_{Y}^{i}\right)^{\rho^i}\right]=1-P\left(\sigma_{eqv}^{i}\right) \tag{25}$$

and then, integrating previous approaches (Sornette 1989, 1992; Hemmer and Hansen 1992) in the proposed model, axial force and torque for the generic $i-th$ layer at this stage can be written as

$$\overline{F}^{i} = N_i \times \left(T_i \sin\alpha_i + S'_i \cos\alpha_i\right) \times \exp\left[-\left(\sigma_{eqv}^{i}/\sigma_{Y}^{i}\right)^{\rho^i}\right] \tag{26}$$

and

$$\overline{M}_t^{i} = N_i \times \left(H_i \sin\alpha_i + G'_i \cos\alpha_i + T_i r_{hi} \cos\alpha_i - S'_i r_{hi} \sin\alpha_i\right) \times \exp\left[-\left(\sigma_{eqv}^{i}/\sigma_{Y}^{i}\right)^{\rho^i}\right] \tag{27}$$

where σ_{eqv}^{i} denotes the equivalent stress in the wire of the generic $i-th$ layer (see Eq. (23)). Finally, from Eq.(22) and for a prescribed number m of strand layers, it follows that

$$\overline{F} = \sum_{i=1}^{m} \overline{F}^{i} \tag{28}$$

$$\overline{M}_t = \sum_{i=1}^{m} \overline{M}_t^{i} \tag{29}$$

which, in terms of stiffness coefficients $k^i_{\alpha\beta}$, one can explicitly rewrite as

$$\overline{F} = \varepsilon \times \sum_{i=1}^{m} k^i_{\varepsilon\varepsilon} \exp\left[-\left(\sigma^i_{eqv} / \sigma^i_Y \right)^{\rho^i} \right] + \varphi \times \sum_{i=1}^{m} k^i_{\varepsilon\varphi} \exp\left[-\left(\sigma^i_{eqv} / \sigma^i_Y \right)^{\rho^i} \right] \tag{30}$$

$$\overline{M}^i_t = \varepsilon \times \sum_{i=1}^{m} k^i_{\varphi\varepsilon} \exp\left[-\left(\sigma^i_{eqv} / \sigma^i_Y \right)^{\rho^i} \right] + \varphi \times \sum_{i=1}^{m} k^i_{\varphi\varphi} \exp\left[-\left(\sigma^i_{eqv} / \sigma^i_Y \right)^{\rho^i} \right] \tag{31}$$

a form which can be helpfully utilized in analytical approaches as well as in numerical step-by-step procedures to solve the problem of the progressive collapse of wires, up to the overall failure of hierarchical strands with helically organized microstructure.

Note that, in the limiting case of bundles made by two types of straight wires (i.e. $\alpha_1 = \pi/2$ and $\alpha_2 = \pi/2$) Eq. (30) reduces to the formula already obtained by some of the present authors in a previous work (Bosia et al. 2012), i.e.:

$$\lim_{\substack{\alpha \to \pi/2 \\ m \to 2}} \overline{F} = \varepsilon \times \left\{ A_1 E_1 N_1 \exp\left[-\left(\sigma^{(1)}_{eqv} / \sigma^{(1)}_Y \right)^{\rho^{(1)}} \right] + A_2 E_2 N_2 \exp\left[-\left(\sigma^{(2)}_{eqv} / \sigma^{(2)}_Y \right)^{\rho^{(2)}} \right] \right\} \tag{32}$$

in which the coupling torsion-elongation obviously disappears and Eq. (16) in the above work is obtained.

4. *In silico* FE-based simulations

To validate analytical solutions, Finite Element (FE) analysis has been performed on selected hierarchically organized strand geometries. Standard 20-node brick (parallelepiped) elements with three translational degrees of freedom for each node have been adopted, obtaining overall a mesh of about 28.000 elements. This number can vary slightly as a function of the selected hierarchical geometry to be implemented. Nonlinear analysis has thus been performed by taking into account the geometric updating of wires at each step of the numerical calculation. For all the systems a total volume per unit length $V_{\text{tot}} = 100 \text{ mm}^2$ has been assumed and boundary conditions have been assigned by imposing an overall stretch of up to 2% to the strands, and simultaneously imposing zero twisting at the strand extremities, i.e. $\varphi = 0$. The wire material is linearly elastic up to its yielding point, at which point brittle failure is assumed to occur. The mechanical properties are additionally characterized by a probabilistic distribution of the wire strength. In particular, to reproduce this statistical feature in the FE models, different strength values have been assigned to the elements of each wire by launching a random generation procedure based on the Weibull distribution with relative probability density function described by Eq. (24). For the cases considered below, in the numerical analysis it is assumed that each single wire breaks when the maximum value of a selected equivalent stress σ^{FE}_{eqv} equals the corresponding prescribed limit threshold. The equivalent stress σ^{FE}_{eqv} in a single wire is then evaluated using the von Mises yield criterion through the following relation

$$\sigma^{FE}_{eqv} = \left(\sum_{e=1}^{e_w} \sigma^e_{eqv} \times v^e \right) \times \left(\sum_{e=1}^{e_w} v^e \right)^{-1} \tag{33}$$

where v^e is the volume of the generic element of the wire, σ^e_{eqv} is the von Mises stress of the element and e_w is the total number of elements constituting the mesh of the selected wire.
Finally, since they are of possible interest for many engineering applications, the toughness values

$$\Psi^F_{\varphi=0} = \frac{1}{V_{\text{tot}}} \int_0^{\varepsilon_f} \overline{F} d\varepsilon \tag{34}$$

have been analytically and numerically computed to estimate how this mechanical property changes with the hierarchical configurations in bundles of wires helically arranged, for prescribed materials and fixed volume, V_{tot} being the total volume per unit length of the strand according to Eq. (35).

5. Results

Although the proposed model allows to take into account different mechanical properties (stiffness and strength) for each wire, as explicitly detailed in the equations above, the analyses were performed by making reference to the same threshold stress. This choice is motivated to the fact that we need to show how the strand hierarchical microstructure can (alone) lead to unequal load sharing, and a different assignment of strength to the wires in a strand would have obscured the crucial role played by the geometry in influencing this heterogeneous stress distribution.
Therefore, in order to show the predictive capabilities and reliability of the proposed *hybrid* (deterministic-probabilistic) modelling approach in predicting how a statistical distribution of material properties, helical structure and hierarchical organization of strands all combine to determine the overall elastic and failure mechanical response of bundles of wires, a wide campaign of *in silico* simulations has been conducted, by exploring different possible strand microstructural configurations and making use of Eqs. (30) and (31).
Analytical solutions are compared to Finite Element (FE) analysis for the chosen hierarchically organized strand geometries. These are generated - without loss of generality - by combining two elemental archetypes, i.e. self-similar (SS) and multi-layer (ML) strand paradigms. An illustrative image of this generation criterion is shown in Figure 3.
In particular, as illustrated in Figure 3, the analysis has been performed by taking into account the following strand configuration types: simple straight strands (2 layers, e.g. 1 core and 1 external layer of wires), multilayered straight strands (3 to 5 layers, e.g. 1 core and 2 to 4 external layers respectively), two-level hierarchical simple straight (HSS) strands (2 layers at level 1 and 2 layers at level 2), and two-level hierarchical multilayered straight (HML) strands (3 layers at the level 1 and 3 layers at the level 2). Also, to quantitatively compare the results in terms of generalized stress-strain behaviour up to failure, as well as in terms of elongation-twisting coupling, specific geometrical constraints have been established to govern the strand generation rules for all the cases investigated. In particular, Eq. (21) has been used to relate the number of wires in each external layer to the wire radii in order to fill the cross-sectional area of the layer. Additionally, each helically wound wire in a strand is characterized by the same pitch length, all the wires are made of the same material with failure probability ruled by the same distribution function, and the total volume per unit length of the strand is imposed as a constant using the formula

$$V_{\text{tot}} = \sum_{i=1}^{m} \frac{N_i \pi R_i^2}{\sin \alpha_i} \tag{35}$$

The "volume per unit length" has obviously the dimensions of an area, but it is greater than the "nominal cross section of the strand", its projection on the plane whose normal is co-axial with the strand axis *de facto* representing the sum of the actual cross-sectional areas of the wires.
In the case of different strand geometries and hierarchies, results have first been obtained analytically and then compared with the results of numerical FE-based simulations: they are synoptically collected in Figures 4 and 5, respectively, and the corresponding details relative to the geometrical parameters adopted for the analyses are reported in Tables 1 and 2.
As a matter of fact, the obtained analytical results - confirmed by the numerical FE-based outcomes - highlight that neglecting elongation-torsion coupling implies a significant overestimation of the actual axial force experienced by stretched bundles and a drastic underestimation of the torque, in the cases (often found in real situations) of clamped ends (see Figures 4 and 5).
Furthermore, by changing hierarchical architectures (i.e. the number of wires and/or their assembly in the bundle for a constant volume, mean wound angle and material properties) no relevant differences from an engineering point of view were found in terms of axial force versus elongation, while - on the contrary - differences up to 100% in terms of torque peaks were highlighted as a function of the wire wrapping and arrangement. This behavior thus affects the way in which shear stresses combine with normal stresses at the single wire level, in turn modifying the mechanical energy stored by bundles during loading processes and finally influencing toughness and mechanisms of rupture (see Figures 4, 5, and 7) by creating prestress conditions prodromal to elastic-plastic buckling failure modes. The latter cannot be predicted adopting simpler ELS models.
Finally, experimental tests (for axial tensile load) were performed on three actual strands of steel wires all arranged in the hierarchical way illustrated in the Figure 4 (top-right), thus constituted by a central core and two surrounded layers of respectively five and eleven wires, whose dimensions - for fabrication requirements - are smaller than those analyzed in the simulations, the structural configuration however preserving the same geometry of the "multilayered straight stand 11X5X1" of the above recalled Figure 4 (top-right). The strand sizes and the other specifications are reported in the caption of the new Figure 6 (the previous Figure 6 has been renumbered as Figure 7) in the revised version of the paper. Although limited to these three tests, comparison between experimental results and theoretical outcomes from the proposed Unequal Load Sharing (ULS) model shows a good agreement for the most part of the force-strain profile, the final tract of the softening predicted by the theory exhibiting a discrepancy with respect to the actual behavior of the tested strands, as a result of their more complex rupture modes which were not included in the theoretical model. Nevertheless, it is worth to highlight that the relevant quantitative and qualitative mechanical behaviors of the strand analyzed seem to encourage the use of the proposed strategy.

5. Discussion and conclusions

By making reference to a hybrid approach in which a Weibull probability function for the material strength is integrated into a deterministic model of a strand, several geometries of hierarchically organized bundles with helically wound wires have been investigated. Analytical and numerical FE analyses have been performed, generating different hierarchical architectures (see Figure 3) and

plotting the results in terms of resultant axial force versus axial elongation of the strands, as well as in terms of torque against axial strain. The results show the effectiveness of the hybrid modeling strategy in capturing both elastic and nonlinear behavior of the structures up to failure, also predicting the coupled twisting-elongation response of the bundles due to the helical wire configurations (Figure 4). The comparison of the analytical results with FE simulations highlights the robustness of the method, as shown in Figure 5 for different strand geometries and statistical Weibull distributions of wire strengths. Additionally, analytically derived maximum axial force (Figure 7A), maximum torque (Figure 7B) and overall strand toughness (Figure 7C) as functions of the helix angle of the outermost layer of wires in multilayered and hierarchical strands have been found for the case of axially stretched strands with twisting locked at the bundle ends. All the results highlight how complex and sometimes unforeseeable responses can be obtained by changing strand microstructure, independently from the statistical distribution of material properties, tracing the ELS hypothesis as a limit case.

As a matter of fact, to faithfully catch the actual post-elastic response of the strand up to its complete failure, several aspects should be additionally taken into account, such as friction, actual constitutive relations governing the exchange of stresses at the interfaces among wires, as well as possible ruptures occurring at single wire level due to instability phenomena induced by the coupling of local twisting/tensile loading. Despite their relevance, these more complex structural responses were considered behind the scope of the present work because they would have required very specific assumptions on how the intrinsic post-elastic properties of the wires combined with the nonlinear mechanical behavior of the material interfaces, which would have moved away the focus from the effect of the strand hierarchical organization on the *unequal* load sharing.

On the basis of the results, the proposed *hybrid* approach, in which the probability of rupture is included into a deterministic mechanical model of a strand constituted by helically-arranged and hierarchically-organized wires, can be usefully employed to study complex bundle architectures under combined axial and torque load conditions, gaining important advantages in terms of accuracy of the results and capability of quantitatively predicting coupled mechanical responses when the ELS hypothesis is no longer applicable.

It is in particular felt that the proposed updated model can be helpfully applied in several fields, from biological to composite materials. Indeed, elongation-torsion coupling is essential to understand the real mechanical behaviour of helically arranged protein filaments in the cytoskeleton and the response of many biological tissues organized in a hierarchical way. In many cases, as in muscles and tendons, the self-similar architecture is a result of multiphysics optimization processes involving overall structure toughness, torsional (and bending) flexibility and nutrient walkway and transport phenomena throughout vessel and micro-channels networks regulated by the interplay between (interstitial fluid) pressure gradients and *in situ* deviatoric stress states. Moreover, with respect to man-made materials, for instance in cord-rubber composites for tire applications, modelling axial force-torque coupling can help to analyse and gaining insights into the shear stresses transferred across reinforcement-matrix interfaces, thus paving the way for new possible design optimization strategies.

Acknowledgements

N. M. P. is supported by the European Research Council (ERC StG Ideas 2011 BIHSNAM n. 279985 and ERC PoC 2015 SILKENE nr. 693670), and by the European Commission under the Graphene Flagship (WP 14 “Polymer nanocomposites” n. 696656). F. B. is supported by the BIHSNAM grant.

References

Bosia, F., Abdalrahman, T. and Pugno, M.N., 2012. Investigating the role of hierarchy on the strength of composite materials: evidence of a crucial synergy between hierarchy and material mixing. Nanoscale 4, 1200-1207.

Bosia F., Lepore E., Alvarez NT., Miller P., Shanov V., Pugno NM., 2016. Knotted synthetic polymer or carbon nanotube microfibres with enhanced toughness, up to 1400 J/g. Carbon 102, 116-125.

Costello, G.A., Philips, J.W., 1976. Effective Modulus of twisted wire cables. ASCE, Journal of the Engineering Mechanics Division 102, 171-181.

Costello, G., 1990. Mechanical models of helical strands. Appl. Mech. Rev. 50, 1-14.

Daniels, H. E., 1945, The Statistical Theory of the Strength of Bundles of Threads, Proc. R. Soc. London, Ser. A 183, 405.

Ghoreishi, S.R., Messager, T., Catraud, P., Davies, P., 2007. Validity and limitations of linear analytical models for steel wire strands under axial loading, using 3D FE model. Int. J. Mech. Sci. 49, 1251-1261.

Hemmer, P. C., and A. Hansen, 1992. The distribution of simultaneous fiber failures in fiber bundles.ASME J. Appl. Mech. 59, 909-914.

Labrosse, M., 1998. Contribution à l’étude du rôle du frottement sur le comportement et la durée de vie des câbles monocouches. PhD thesis, Ecole Centrale de Nantes, France.

Love, A. E. H., 1944. A treatise on the mathematical theory of elasticity, fourth ed. Dover Publications, New York.

Meyers M.A., Chen P., Yu-Min Lin A., Seki Y., 2008, Biological materials: Structure and mechanical properties, Progress in Materials Science, 53 (1), 1-206.

Nawrocki, A., Labrosse, M., 2000. A finite element model for simple straight wire rope strand. Computer & Structures 77, 345-369.

Pan N., 1993, Journal of Materials Science 28, 6107.

Pugno M.N., Bosia F, Carpinteri A, 2008, Multiscale Stochastic Simulations for Tensile Testing of Nanotube-Based Macroscopic Cables, Small 4 (8), 1044-1052.

Pugno, M.N., Bosia, F., Abdalrahman, T., 2012. Hierarchical fiber bundle model to investigate the complex architectures of biological materials. Phys. Rev. E 85, 011903.

Pugno, M.N., 2014. The “Egg of Columbus” for making the world's toughest fibres. Plose One, 9 (4), e93079, (6 pp).

Pradhan S., Hansen A., Chakrabarti B.K., 2010, Failure processes in elastic fiber bundles, Rev. Mod. Phys. 82, 499

Ramsey, H., 1988. A theory of thin rods with application to helical constituent wires in cables. Int. J. Mech. Sci. 30, 559-570.

Ritchie, R. O. 2011. The conflicts between strength and toughness. Nature Mater. 10, 817–822

Sornette, D., 1989. Elastic and failure of a set of elements loaded in parallel. J. Phys. A **22**, L243-L250.

Sornette, D., 1992. Mean-field solution of a block-spring model of earthquakes. J. Phys. I **2**, 2089-2096.
Utting, W., Jones, N., 1987. Response of wire rope strands to axial tensile loads. Part I: Experimental results and theoretical predictions. Int. J. Mech. Sci. 29 (9), 605-661.
Weibull, W., 1951. A statistical distribution function of wide applicability. ASME J. Appl. Mech. 18, 293–297.

Table of symbols

R_i	wire radius
α_i	angle of the helical wrapping of the wires
r_i	radius of the helical wrapping of the wires
p_i	pitch of the helical wrapping of the wires
E_i	Young's moduli of the wire material
ν_i	Poisson's ratio of the wire material
λ_i	first Lamé moduli of the wire material
μ_i	second Lamé moduli of the wire material
F	tensile axial force
M_t	torque
ε	strand elongation
φ	strand twisting per unit length
N_i	number of wires in the generic $i-th$ layer of the strand.
L_0, L	strand length in initial and stressed configuration.
$\Delta\Theta$	twist angle between two strand cross sections at a distance L_0
κ_i, κ'_i	wire curvatures
τ_i	wire axial twist
ε_i	wire axial deformation
δr_i	radial deformation of the helix radius
S_i, S'_i	wire shear forces
T_i	wire tensile force
G_i, G'_i	wire bending moments
H_i	wire torque
I_i	wire cross-sectional moment of inertia
J_i	wire cross-sectional polar moment of inertia
A_i	wire cross-sectional area
F_i	axial force on the generic $i-th$ layer
M_t^i	twisting moment on the generic $i-th$ layer
σ_3^i	wire tensile stress
$\tau_{\max}^i$	wire maximum shear stress
$\sigma_{\max}^i$	maximum normal stress due to the bending moment on the wire
σ^i	wire normal stress
τ^i	wire shear stress
σ_{eqv}^i	equivalent wire stress
J_2^i	wire second deviatoric stress invariant
σ_Y^i	wire reference yield stress
ρ^i	Weibull shape factor for the wire material
$k_{\alpha\beta}^i$	wire generic strand stiffness component
$\overline{F}$	resultant strand axial force
$\overline{M}_t$	resultant strand torque
$\overline{F}^i$	emerging axial force in the generic $i-th$ layer
$\overline{M}_t^i$	emerging twisting moment in the generic $i-th$ layer
V_{tot}	total volume per unit length of the strand
σ_{eqv}^{FE}	maximum value of the equivalent stress in the wire
v^e	volume of the single finite element of the wire model
e_w	number of elements in the FE wire model
σ_{eqv}^e	von Mises stress of the single finite element of the wire model
$\Psi_{\varphi=0}^F$	expected strand toughness
m	number of strand layers

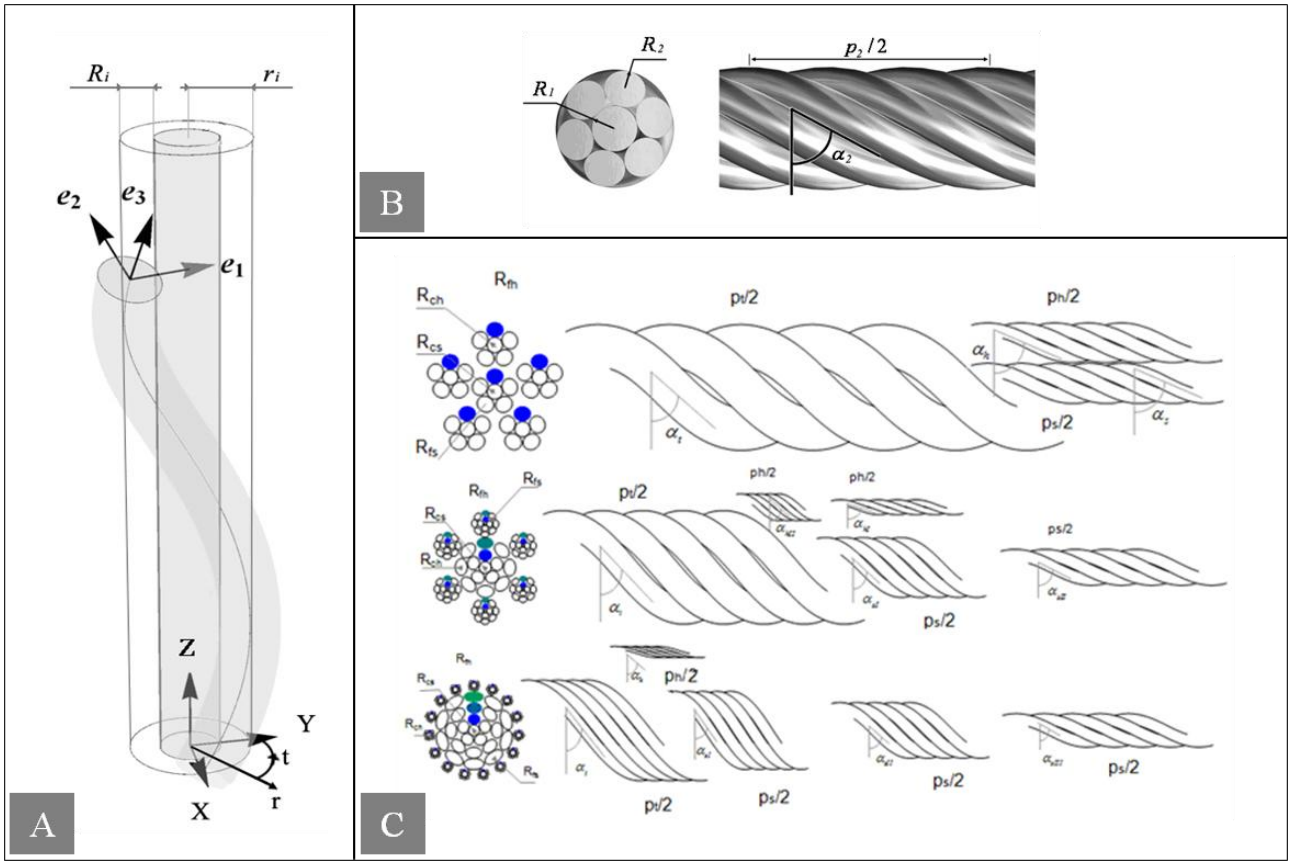

Figure 1: A) Sketch of a generic strand unit with helically arranged wires and the two considered reference coordinate systems. B) Simple $(6+1)$ straight strand: cross-section and lateral view. C) Representation of different possible arrangements of wires and cores in a hierarchically organized strand (see text for details). In the Figure, z is the strand axis, α_i is the helical angle of the wire belonging to the i-th layer of wires, r_i represents the distance from the strand axis of the generic layer of wires and R_i is the corresponding cross section wire radius.

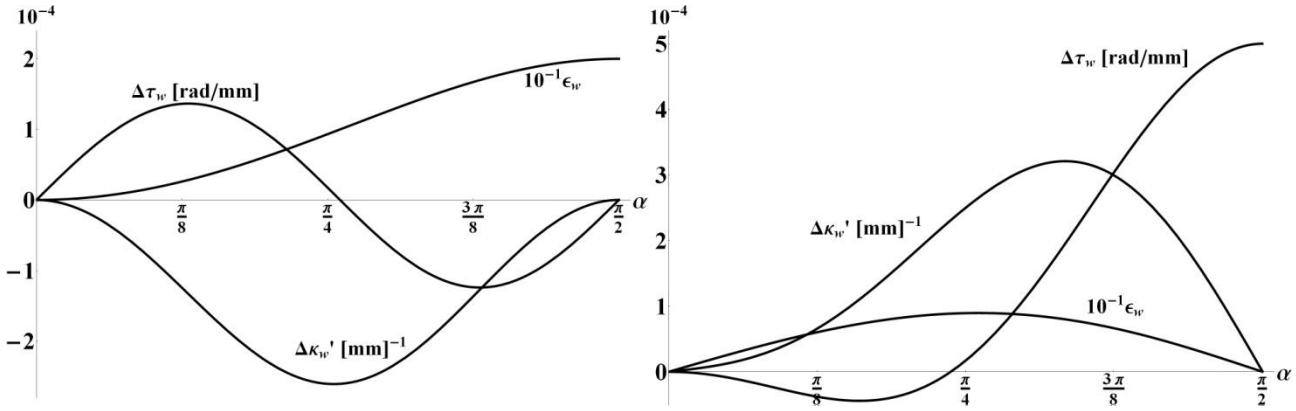

Figure 2. Kinematics of a single wire in a strand under axial displacement, i.e. local elongation ε_w, curvature $\Delta\kappa'_i$ and torsion $\Delta\tau_i$ for varying helical angle α. *Left*: fully clamped end conditions; strand axial load $F = 40\,k\text{N}$, strand axial torsion per unit length $\varphi = 0$. *Right*: torque-free conditions; strand axial load $F = 40\,k\text{N}$, strand axial torque $M_t = 0$ (Strand parameters: $R_c = 1.97\text{ mm}, R_w = 1.865\text{ mm}, E = 197.9\text{ GPa}, \nu_c = 0, \nu_w = 0.3$).

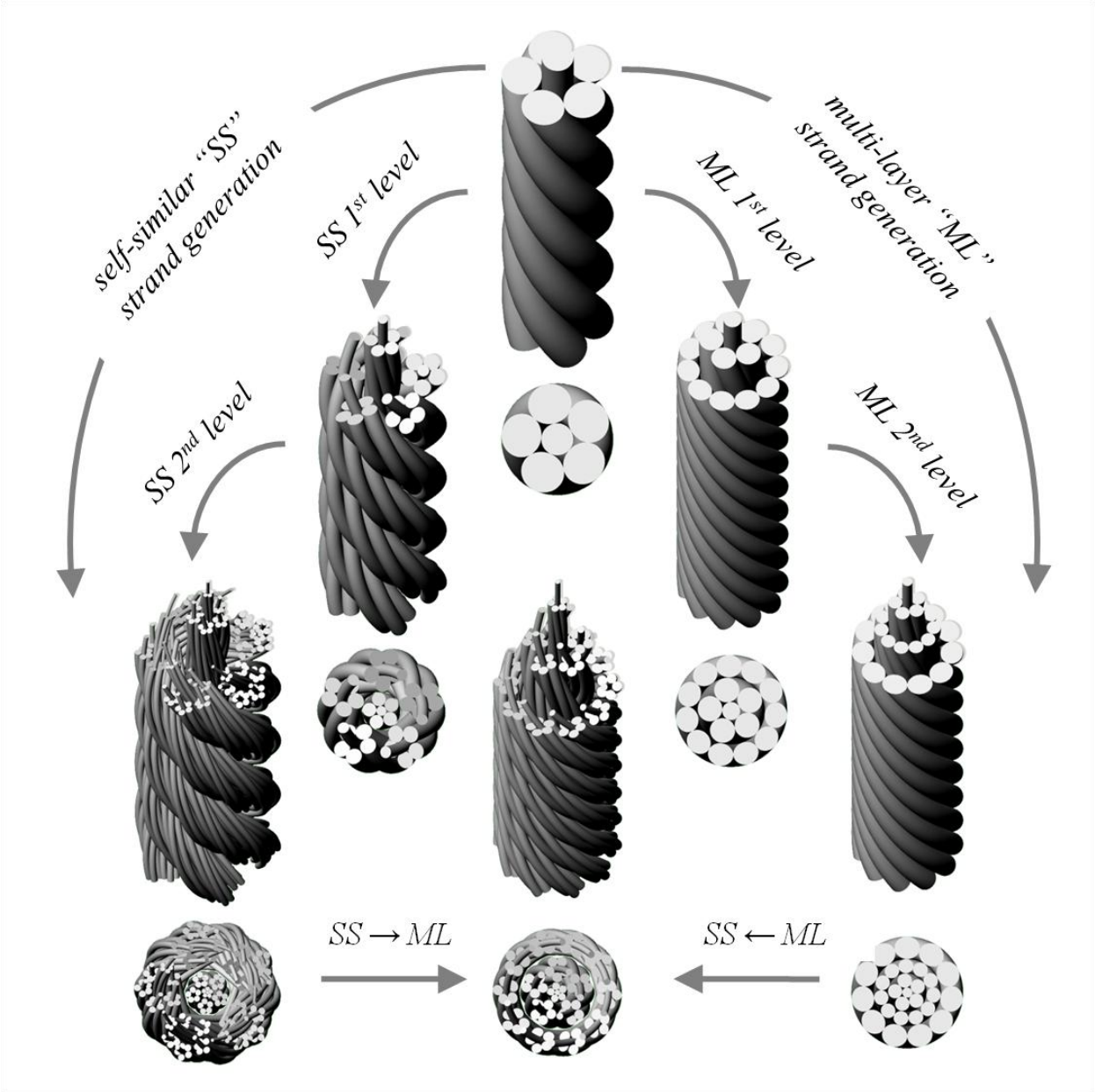

Figure 3. Hierarchical strands with helically arranged wires: possible rules for assembling wires and strand layers to generate hierarchical structures starting from two main assembly procedures, i.e. self-similar (SS) and multi-layer (ML) ones, finally combined to obtain complex bundle geometries.

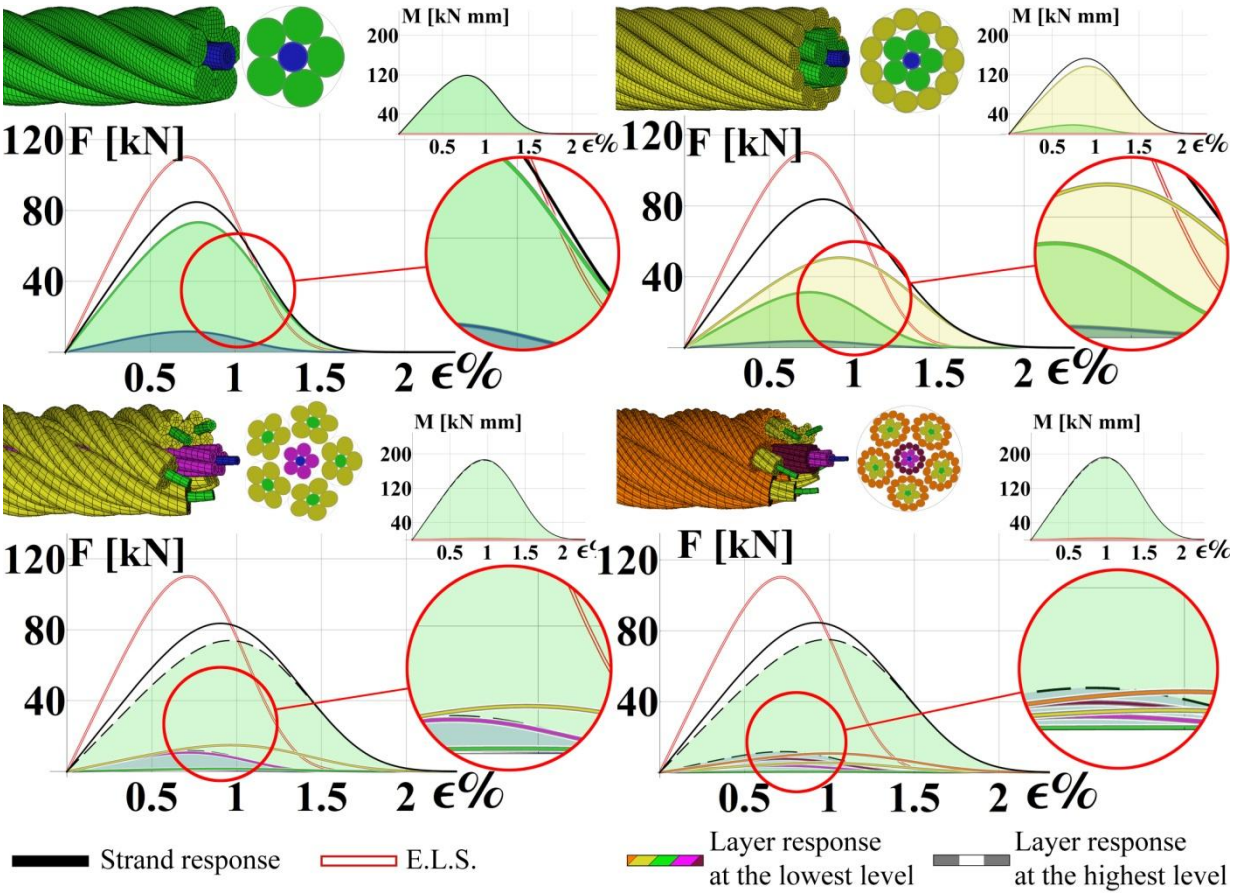

Figure 4. Analytical models and results in terms of tensile force F and torque M vs strain up to failure for a simple straight strand 5X1 (*top-left*), a multilayered straight strand 11X5X1 (*top-right*), a hierarchical strand 5X1-5X1 (*bottom-left*) and a hierarchical strand 5X1-12X5X1 (*bottom-right*). Geometrical parameters are reported in Table 1. For wires, mechanical parameters are Young's modulus $E_i = 197900\,\text{MPa}$, Poisson's ratio $\nu_i = 0.3$, Weibull scale factor $\sigma_Y^i = 2000\,\text{MPa}$ and Weibull shape factor $\rho^i = 4$. Theoretical results from the hybrid probabilistic-deterministic model for a tensile test are illustrated for the case in which twisting is not permitted. The black lines refer to the overall strand response, the coloured lines refer to the response of the single layer at the lowest hierarchical level in the strand (illustrated using the corresponding colour in the graphics above), the grey dashed lines denote the single layer response at the highest hierarchical level in the strand (shaded with the blue, green and yellow colour in case of core, 1st and 2nd external layer respectively), while the red thick lines indicate the results obtained from ELS hypothesis, here obtained as special case of the proposed theory as in Eq. (32). Note that ELS does not capture the coupling between torsion and elongation.

Strand Type		wire radii						layer helix angles				
5X1		core radius $R_1 = 1.83\,mm$			layer 2 wire radius $R_2 = 2.29\,mm$			layer 2 helix angle $\alpha_2 = 66.7^\circ$				
11X5X1		core radius $R_1 = 1.03\,mm$			layer 2 wire radius $R_2 = 1.40\,mm$		layer 3 wire radius $R_3 = 1.28\,mm$	layer 2 helix angle $\alpha_2 = 75.7^\circ$		layer 3 helix angle $\alpha_3 = 61.8^\circ$		
5X1-5X1		1st level -core			1st level -layer 2			1st level -	1st level -core		1st level -layer 2	
		core radius $R_{11} = 0.57\,mm$	layer 2 wire radius $R_{12} = 0.80\,mm$		core radius $R_{21} = 0.68\,mm$	layer 2 wire radius $R_{22} = 0.95\,mm$		layer 2 $\alpha_{12} = 81.9^\circ$	layer 2 angle $\alpha_{21} = 63.7^\circ$		layer 2 \angle $\alpha_{22} = 80.3^\circ$	
5X1-12X5X1	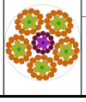	1st level -core			1st level -layer 2			1st level -	1st level -core		1st l.-layer 2	1st l.-layer 3
		core radius $R_{11} = 0.33\,mm$	layer 2 wire radius $R_{21} = 0.40\,mm$	layer 3 wire radius $R_{22} = 0.95\,mm$	core radius $R_{23} = 0.52\,mm$	layer 2 wire radius $R_{12} = 0.47\,mm$	layer 3 wire radius $R_{13} = 0.43\,mm$	layer 2 angle $\alpha_2 = 63.7^\circ$	layer 2 angle $\alpha_{11} = 85.2^\circ$	layer 3 angle $\alpha_{12} = 80.0^\circ$	layer 2 angle $\alpha_{21} = 84.2^\circ$	layer 2 angle $\alpha_{22} = 77.9^\circ$

Table 1. Strand geometrical parameters of the models illustrated in Figure 4.

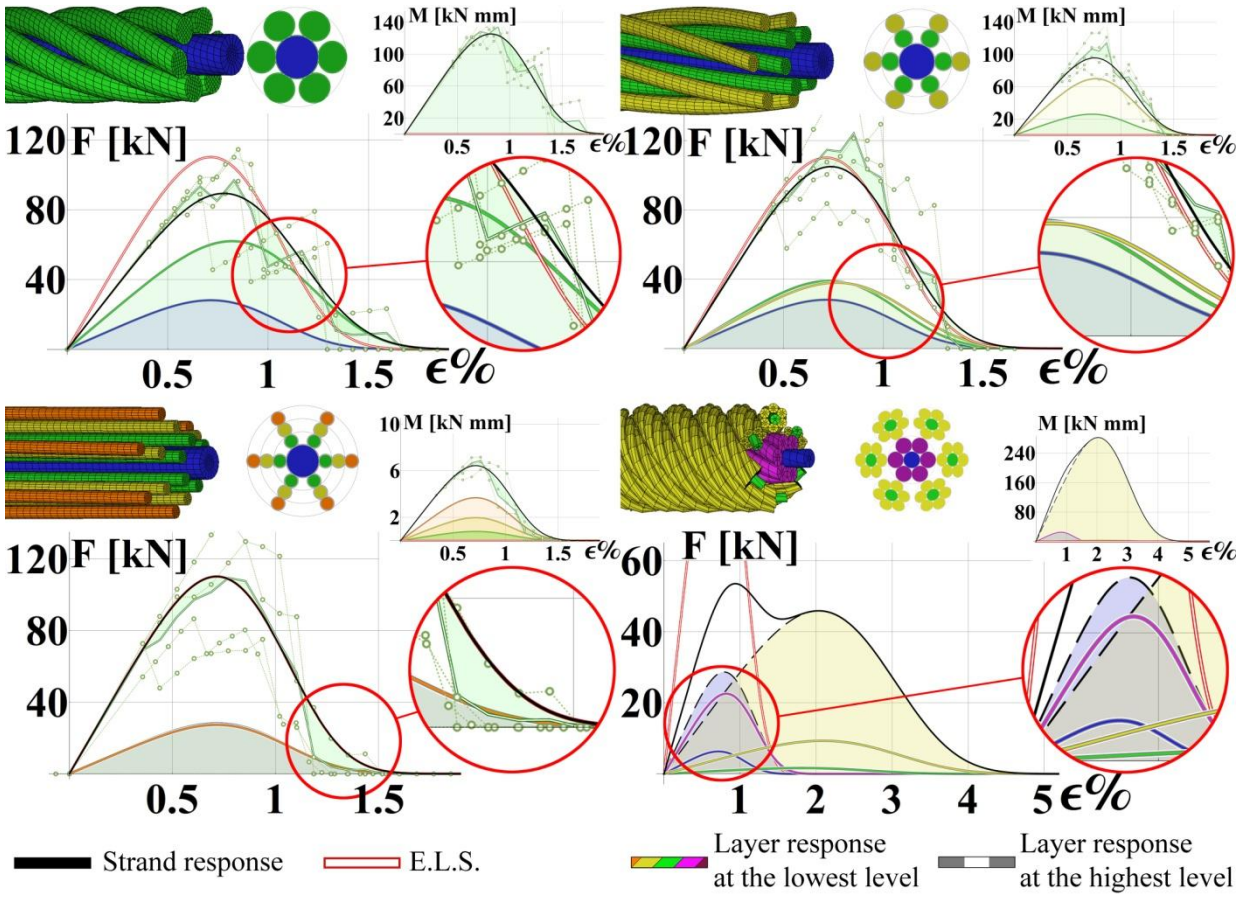

Figure 5. Analytical and FE models with results (axial force F and torque M versus elongation ε) for a simple straight strand 6X1 (*top-left*), a multilayered straight strand 6X6X1 (*top-right*), a multilayered straight strand 6X6X6X1 (*bottom-left*) and a hierarchical strand 6X1-6X1 (*bottom-right*). Geometrical parameters are reported in Table 2, while wire material parameters are those already indicated for Figure 4. Results for a tensile test are illustrated for the case in which twisting is not permitted. The black lines refer to the overall strand response, the coloured lines refer to the response of the single layer at the lowest hierarchical level in the strand (illustrated using the corresponding colour in the graphics above), the grey dashed lines denote the single layer response at the highest hierarchical level in the strand (shaded with the blue, green, yellow and red colour in case of core, 1st, 2nd and 3rd external layer respectively), while the red thick lines indicate the results obtained from ELS hypothesis, here obtained as special case of the proposed theory as in Eq. (32). Note that ELS does not capture the coupling between torsion and elongation.

Strand Type		wire radii				layer helix angles		
1X9	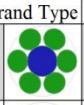	core radius $R_1 = 2.85\,mm$		layer 2 wire radius $R_1 = 1.90\,mm$		layer 2 helix angle $\alpha_2 = 66.7^\circ$		
1X6X9		core radius $R_1 = 2.85\,mm$		layer 2 wire radius $R_2 = 1.39\,mm$	layer 3 wire radius $R_3 = 1.39\,mm$	layer 2 angle $\alpha_2 = 80.9^\circ$	layer 3 angle $\alpha_3 = 75.2^\circ$	
1X6X9X9		core radius $R_1 = 0.24\,mm$	layer 2 wire radius $R_2 = 0.23\,mm$	layer 3 wire radius $R_3 = 0.66\,mm$	layer 4 wire radius $R_4 = 1.90\,mm$	layer 2 angle $\alpha_2 = 88.9^\circ$	layer 3 angle $\alpha_3 = 86.9^\circ$	layer 4 angle $\alpha_4 = 81.2^\circ$
1X9-1X9		1st level -core		1st level -layer 2		1st level -layer 2 angle $\alpha_{12} = 64.8^\circ$	1st level -core layer 2 angle $\alpha_{21} = 42.7^\circ$	1st l.-layer 2 layer 2 angle $\alpha_{22} = 75.1^\circ$
		core radius $R_{11} = 1.35\,mm$	layer 2 wire radius $R_{12} = 1.16\,mm$	core radius $R_{21} = 0.73\,mm$	layer 2 wire radius $R_{22} = 0.69\,mm$			

Table 2. Strand geometrical parameters of the models illustrated in Figure 5.

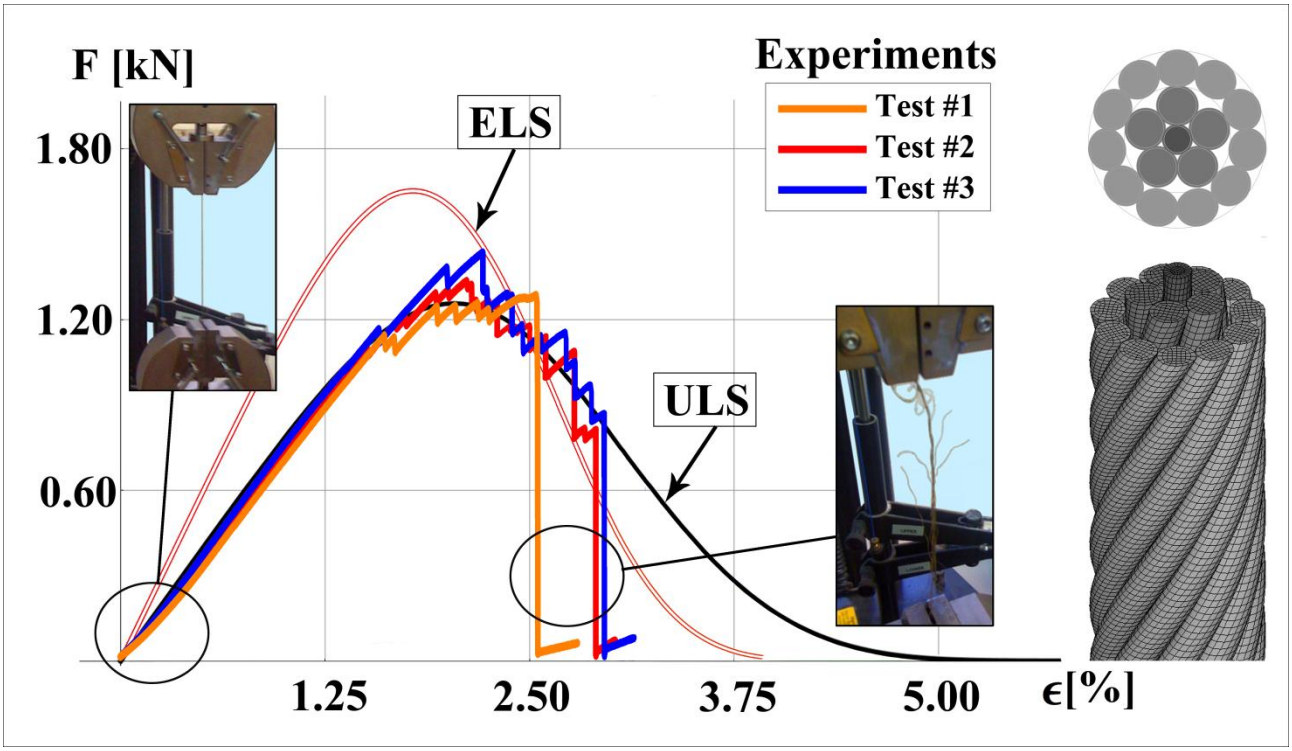

Figure 6. Analytical results for ELS (red curve) and ULS (black curve) in terms of tensile force F versus axial strain up to failure for a multilayered straight strand 11X5X1. The filament diameters are the same for both core and all the wires of the two strand layers and are equal to 0.165 mm, Young moduli and Poisson ratios of the wires, as well as Weibull factors, being instead the same of those adopted in the simulations illustrated in Figures 4 and 5.

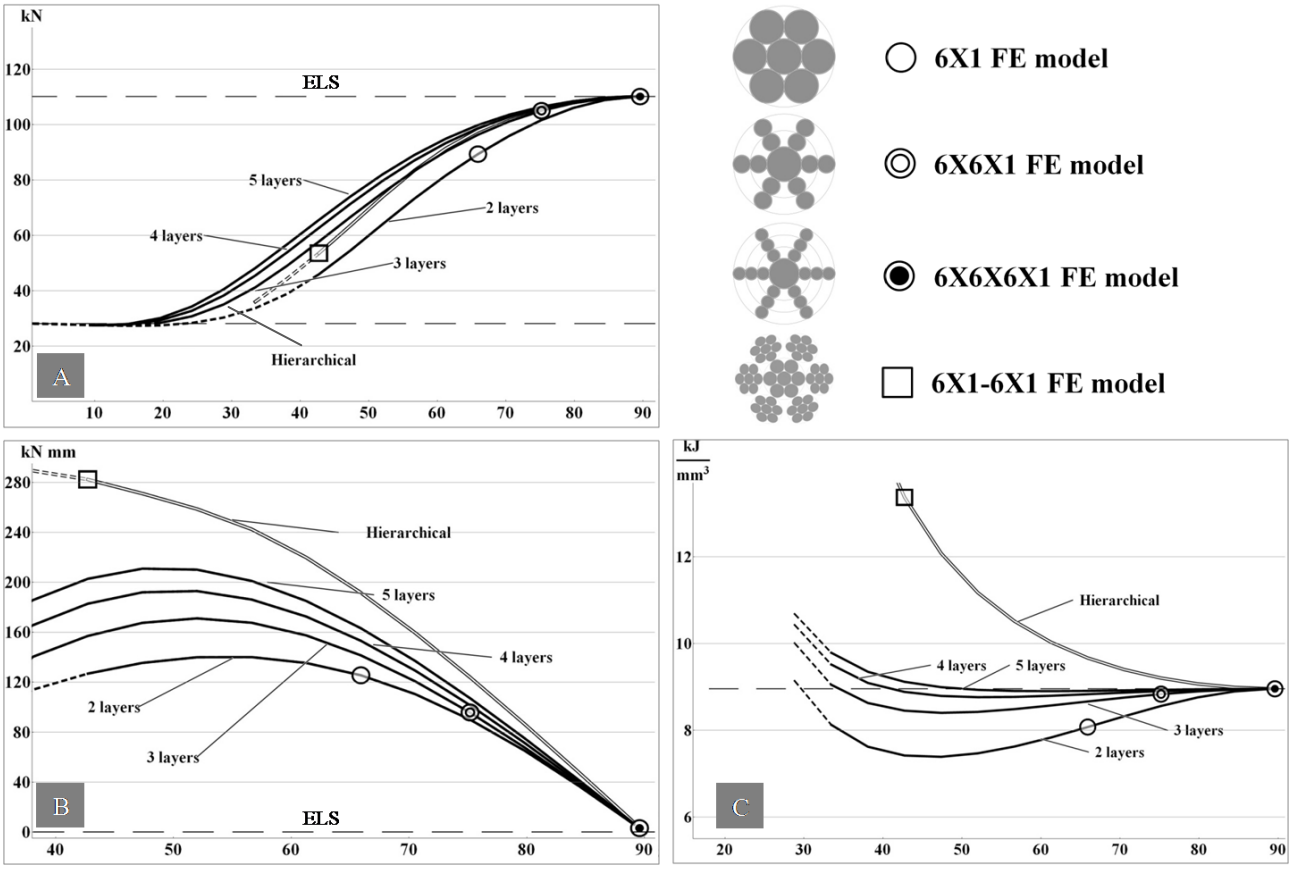

Figure 7. Analytically derived maximum axial force (A), maximum torque (B) and overall strand toughness (C) in the case of axially stretched strands (with twisting locked at the extremities) as functions of the helix angle of the outermost layer. The results have been obtained by performing the analyses on several types of multilayer strands with different number of layers (dashed portions of the lines refer to strand configurations that do not obey the condition (21)). The horizontal dashed line indicates the results obtained from ELS, say in the limit case of Eq. (32) while the markers highlight the FE solutions illustrated in detail in Figure 5.